*Desalination and Water Treatment*
www.deswater.com

doi: 10.1080/19443994.2015.1096834

57 (2016) 19443–19455
September

Taylor & Francis
Taylor & Francis Group

# A multifunctional nanocomposite pectin thorium(IV) tungstomolybdate for heavy metal separation and photoremediation of malachite green

Gaurav Sharma[a,*], Mu. Naushad[b], Deepak Pathania[a], Amit Kumar[a]

[a]*School of Chemistry, Shoolini University, Solan 173212, Himachal Pradesh, India, emails: gaurav8777@gmail.com (G. Sharama), dpathania74@gmail.com (D. Pathania), mittuchem83@gmail.com (A. Kumar)*
[b]*Department of Chemistry, College of Science, Bld.#5, King Saud University, Riyadh, Saudi Arabia, email: mnaushad@ksu.edu.sa*

Received 19 April 2015; Accepted 14 September 2015

ABSTRACT

The nanocomposite pectin thorium(IV) tungstomolybdate (Pc/TWM) has been prepared by incorporating pectin biopolymer within thorium(IV) tungstomolybdate, precipitated at 80°C. The synthesized nanocomposite material was characterized using scanning transmission electron microscopy, transmission electron microscopy, scanning electron microscopy, X-ray diffraction analysis, and Fourier transform infrared spectroscopy. The binary mixture separations of heavy metal ions have been performed proficiently on the columns of Pc/TWM. The synthesized nanocomposite was exploited for removal of malachite green from the aqueous system under two set of conditions. The synergistic/adsorptional photocatalysis conditions were found to be more efficient than equilibrium adsorption followed by photocatalysis in the dark. The Pc/TWM also showed promising antibacterial activity against the bacteria, *Staphylococcus aureus*. Thus, the nanocomposite material can be used as an adsorbent for the remediation of harmful metals and dye pollutants from wastewater.

*Keywords:* Nanocomposite; Malachite green; Synergistic/adsorptional; Photocatalysis

## 1. Introduction

The environmental pollution has increased due to hazardous and non-degradable components released from the industries [1–3]. The industrial wastewater contains water pollutants such as surfactants, phenols, buffers, dyes, metals, scouring agents, bleaches, caustic compounds, acids, and xylenes. [4–7]. The various methods employed for remediation of harmful pollutants include adsorption, ion exchange, chemical precipitation, photocatalysis, etc. The researchers are exploring a number of remediation materials which includes agricultural waste, biopolymers, carbon nanotubes, graphene, metal oxides, biochar, etc. [8–14]. The advanced nanocomposites play a vital role in the environmental protection due to their specificity, selectivity, and a wide range of usability [15–17]. The efforts have been made to improve the chemical, mechanical, and thermal stabilities of composites so they can be used as a selective material for removal of heavy metal ions and dyes [18–24]. In composite materials, two uniquely different materials possessing completely different properties have been joined for developing materials having better granulometric properties than its constituent materials. Beyond additional advantages, composite materials have been more stable at intense radiation fields and at high temperature [25,26]. The composite materials

*Corresponding author.

based on inorganic and organic constituents have enhanced properties such as better thermal stability, chemical stability, selectivity, etc. [27,28]. Hence, these materials have been applied in dissimilar fields such as ion-selective electrodes, antibacterial activity, biomolecular separations, catalysis, ion potentiometric sensor, hydrometallurgy, and chromatographic separations [29–32]. The inclusion of biopolymer part into an inorganic component to form composite materials has been useful for removal and recovery of heavy metals and harmful dyes from the wastewater system. Thus, different materials have been exploited for the treatment of dye waste from the aqueous system.

In the present work, the nanocomposite pectin thorium(IV) tungstomolybdate has been exploited for removal of malachite green and heavy metals from the water system. The nanocomposite material has also been studied for its antimicrobial activity against *Staphylococcus aureus*.

## 2. Materials and method

### 2.1. Reagents and instruments

Thorium nitrate, methylene blue, sodium tungstate (LobaChemie Pvt. Ltd, Mumbai, India), and sodium molybdate (CDH Pvt. Ltd, New Delhi, India) were used. A scanning electron microscope (Quanta 250, FEI Make Mode no. D9393), UV–vis spectrophotometer (Systeronics 2202), and water bath incubator shaker were used.

### 2.2. Preparation of reagents

The 0.05 M $ThNO_3{\cdot}6H_2O$ solution was prepared in 0.1 N $HNO_3$, 0.05 M $Na_2WO_4{\cdot}2H_2O$ and 0.05 M $Na_2MoO_4{\cdot}2H_2O$ were prepared in demineralized water (DMW).

### 2.3. Synthesis of pectin thorium(IV) tungstomolybdate

The composite was synthesized by the sol–gel method as discussed in the literature [33]. In this, the pectin gel was added to the inorganic precipitate of thorium(IV) tungstomolybdate prepared by mixing equimolar concentration of thorium nitrate, sodium tungstate, and sodium molybdate with constant stirring at 80˚C. The pH of the solution was adjusted at ~1 by adding 0.1 N $HNO_3$. The resulting mixtures were kept overnight for digestion. Finally, the precipitates were filtered, dried, and transformed into $H^+$ form by immersing the material in 1 N $HNO_3$ for 24 h.

### 2.4. STEM, TEM, SEM, XRD, and FTIR studies

Scanning transmission electron microphotographs of pectin thorium(IV) tungstomolybdate nanocomposites were obtained using an LEO 435 VP instrument, and transmission electron microphotographs were recorded using transmission electron microscope. The physical nature of Pc/TWM was obtained by an XPERT-PROX-ray diffractometer using Cu Ka radiation. The Fourier transform infrared spectroscopy (FTIR) spectrum of Pc/TWM was recorded using KBr pellets method on a Nicolet 5700 FTIR spectrometer.

### 2.5. Band gap studies

In this method, a dispersion of nanocomposite was prepared in distilled water and ultrasonicated for 1 h in an ultrasonic cleaner. The UV–vis spectra were noted using double beam spectrophotometer.

A curve of absorbance vs. wavelength has been plotted. From the absorbance values, absorption coefficient ($\alpha$) was calculated using the formula [34]:

$$\alpha = 2.303\,A/l \tag{1}$$

where $A$ = absorbance and $l$ = length of light path through the sample in cm.

The UV–vis spectral data has been used for the determination of optical band gap (i.e. the difference between the conduction band energy and the valence band) using the Tauc relation [35,36]:

$$\alpha h\nu = A(h\nu - Eg)n \tag{2}$$

where $\alpha$ is the absorption coefficient and $d$ is the thickness of the sample, $Eg$ is the energy band gap, $n$ (1/2, 1, 2) is a constant dependent on the degree of transition, $n = 1/2$ for direct band gap semiconductors, and $h\nu$ is incident photon energy.

The band gap was assessed by plotting $h\nu$ vs. $(\alpha h\nu)^2$ and extrapolating the tangent on the $X$-axis (Tauc Plots).

### 2.6. Quantitative separations of metal ions from synthetic binary mixtures

Some important quantitative separations of metal ions were performed on columns of Pc/TWM. 1.0 g of nanocomposite in $H^+$ form was taken in glass column of internal diameter 0.6 cm and a height of 35 cm. The washing of the column was done with double-distilled water and then with the suitable solvent. The mixtures of metal ions, each with initial concentration 0.1 M

were loaded and allowed to pass through the column at a flow rate of 0.20 mL/min. This mixture was circulated two or three times to ensure the complete absorption of metal ions on the column. The absorbed metal ions were eluted with the suitable solvent of required concentration. The effluent was collected in 10-mL fractions and determined titrimetrically using a standard solution of 0.01 M disodium salt of EDTA [37].

### 2.7. Selective separation of metal ions from synthetic mixtures

The selective separations of metal ions from synthetic mixtures were achieved on columns of Pc/TWM. In this method, 1.0 g of nanocomposite in $H^+$ form was taken in a glass column and washed thoroughly with DMW. The known concentrations of mixtures of different metal ions were passed through the column many times. Then the varying concentrations of suitable solvent were used to elute the metal ions from the columns of the nanocomposite. The amounts of the metal ions were calculated as discussed in the literature[38].The selective separation of $Cr^{3+}$ and $Pb^{2+}$ from synthetic mixture of ($Cr^{3+}$, $Zn^{2+}$, $Ni^{2+}$, $Pb^{2+}$, $Sr^{2+}$, $Mg^{2+}$, and $Cd^{2+}$) for $Cr^{3+}$ and ($Pb^{2+}$, $Zn^{2+}$, $Ni^{2+}$, $Al^{3+}$, $Co^{2+}$, $Mg^{2+}$, and $Fe^{3+}$) for $Pb^{2+}$ was achieved on the column of Pc/TWM nanocomposite. The amount of the $Cr^{3+}$ and $Pb^{2+}$ ions in the mixture was changed keeping the amount of the other metal ions constant in the synthetic mixture.

### 2.8. Photocatalytic activity

The photocatalytic activity of Pc/TWM nanocomposite was explored for the degradation of malachite green in the presence of solar light. The photocatalytic experiments were performed using a double-walled pyrex glass chamber jacketed with thermostatic water circulation to maintain a constant temperature (25°C ± 1). Hundred milligrams of the nanocomposite was added into $2 \times 10^{-6}$ M solution of malachite dye to form slurry [39–41]. The slurry was subjected to the two reaction conditions. Under the first reaction condition, the slurry was kept in dark to attain the adsorption–desorption equilibrium and then exposed to sunlight for further photocatalysis. On the other hand, the slurry was placed directly in sunlight for synergistic adsorption-photocatalysis under the second reaction condition. About 3 mL of the dye solution was withdrawn at various intervals of time and centrifuged to confiscate particles of the nanocomposite. The absorbance was recorded in the range of 300–750 nm and the kinetics for the photocatalytic degradation of MG was investigated at 620 nm. The percent degradation of dye was found as:

$$\%\,\text{Degradation} = \frac{C_o - C_t}{C_o} \times 100 \tag{3}$$

where $C_o$ and $C_t$ are the concentrations of dye at equilibrium and at time $t$.

The rates of photocatalytic degradation of dyes were determined using pseudo-first-order kinetic model as follows:

$$r = -\frac{dC}{dt} = k_{app}t \tag{4}$$

On integrating the above equation, we get:

$$\ln \frac{C_o}{C_t} = k_{app}t \tag{5}$$

where $C_o$ is the concentration of dye before illumination and $C_t$ is the concentration of dye at time $t$, and $k_{app}$ is the apparent rate constant.

### 2.9. Antimicrobial activity against S. aureus

The antimicrobial activity of nanocomposite was determined using Optical density (O.D) method. A colony of *S. aureus* was picked from the overnight nutrient agar plate culture and inoculated into 5 mL of nutrient broth. It was then incubated at 37°C for 24 h. The culture was diluted to $10^{-5}$ CFU/mL (colony forming unit per mL) with NB according to MacFarland standard [33,42]. The different concentrations of Pc/TWM were added into the flasks. The flasks were then incubated in an incubator shaker at 37°C for 24 h. The high rotation was done to minimize aggregation and settlement of the nanocomposite during the incubation period. The positive control was also studied which shows the growth of bacteria in the absence of nanocomposite. After every hour, the O.D of each sample was evaluated using spectrophotometer at 620 nm. The O.D was plotted against time of incubation [43,44].

## 3. Results and discussion

Scanning transmission electron microphotographs (STEM) of pectin thorium(IV) tungstomolybdate composite were shown in Fig. 1(a) and (b). It has been used to understand the surface morphology of the

composite. The STEM photographs of pectin thorium (IV) tungstomolybdate clearly indicated the fibrous nature of the material. This was due to binding of biopolymeric pectin with inorganic moiety. The particle size as evident from STEM and TEM images (Fig. 1(c)) was in the range of 10–30 nm. Thus, the composite material is nanocomposite as the particle size remains in the nano range [33]. The X-ray diffraction (XRD) pattern of Pc/TWM nanocomposite is shown in Fig. 2(a). The low $2\theta$ values confirmed the semi-crystalline nature of the nanocomposite [33]. The scanning electron microscopy (SEM) images of the TWM and Pc/TWM nanocomposites at different magnifications are shown in Fig. 2(b) and (c). The image of inorganic counterpart TWM shows the smooth morphology as shown in Fig. 2(b). Whereas the SEM images of Pc/TWM nanocomposite has a rough surface morphology (Fig. 2(c)). The change in structural morphology of the nanocomposite material indicated the incorporation of pectin into the inorganic counterpart TWM.

The spectrum of Pc/TWM nanocomposite was shown in Fig. 3 [33]. The broad band at 3,351 $cm^{-1}$ represents the water molecules present in the structure of Pc/TWM nanocomposite [29–31]. The peak at 1,023 $cm^{-1}$ was due to C–O bond of pectin [16]. The peaks observed at 951 $cm^{-1}$ may be due to molybdate, and at 798 $cm^{-1}$ may be due to tungstate. The metal-oxide stretching is shown by a peak present at 558 $cm^{-1}$ [19,20,27,33,38]. The peak at 1,700 $cm^{-1}$ was due to C=O of ester and 1,355 $cm^{-1}$ corresponds to stretching bands of free $COO^{-}$ group of pectin [16].

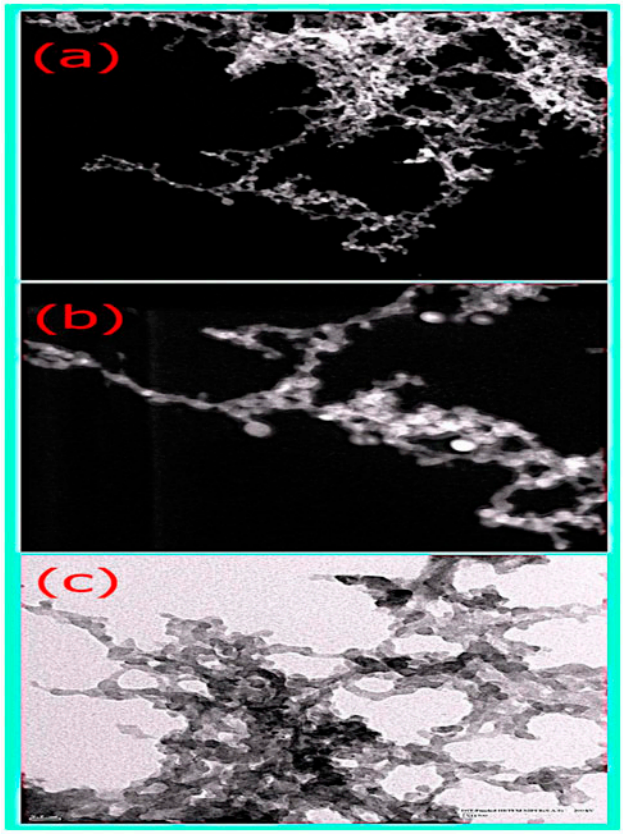


Fig. 1. STEM photographs and (a–b) TEM photographs (c) of pectin thorium(IV) tungstomolybdate [33].

### 3.1. Binary separations

The separation potential of the pectin thorium(IV) tungstomolybdate nanocomposite has been confirmed by achieving some analytically complex binary separations of $Cr^{3+}$, $Pb^{2+}$, $Cu^{2+}$, and $Ca^{2+}$ metal ions from different synthetic binary mixtures of metal ions as $Ni^{2+}$–$Cr^{3+}$, $Ba^{2+}$–$Cr^{3+}$, $Zn^{2+}$–$Cr^{3+}$, $Mg^{2+}$–$Cr^{3+}$, $Ni^{2+}$–$Pb^{2+}$, $Co^{2+}$–$Pb^{2+}$, $Ni^{2+}$–$Cu^{2+}$, and $Ba^{2+}$–$Ca^{2+}$. The successive elution of ions through the column depends on the metal–ligand complex stability. The weakly retained metal ions are thus eluted at the earliest and the strongly retained at the last. The separations are quite sharp, reproducible, and the recovery was quantitative. About 95.95% $Cr^{3+}$, 93.97% $Pb^{2+}$, 91.02% $Cu^{2+}$, and 91.00% $Ca^{2+}$ was recovered in each separation. The detailed results of separations are summarized in Table 1. The salient features of these separations are represented in the chromatograms as shown in Fig. 4.

### 3.2. Separation of $Cr^{3+}$ and $Pb^{2+}$ from synthetic mixture

Selective separation of $Cr^{3+}$ and $Pb^{2+}$ from a synthetic mixture containing $Cr^{3+}$, $Zn^{2+}$, $Ni^{2+}$, $Pb^{2+}$, $Sr^{2+}$, $Mg^{2+}$, and $Cd^{2+}$ for $Cr^{3+}$, and $Pb^{2+}$, $Zn^{2+}$, $Ni^{2+}$, $Al^{3+}$, $Co^{2+}$, $Mg^{2+}$, and $Fe^{3+}$ for $Pb^{2+}$ has been achieved on the column of pectin thorium(IV) tungstomolybdate nanocomposite. The amount of the $Cr^{3+}$ and $Pb^{2+}$ ion in the synthetic mixtures was varied keeping the amount of other metal ions constant. It was indicated that about more than 96% $Cr^{3+}$ and 94% $Pb^{2+}$ metal ions were recovered in each separation. The detailed results are presented in Tables 2 and 3. The adsorption of metal ions onto Pc/TWM nanocomposite is shown in Fig. 5 [33].

### 3.3. Band gap studies

The band gaps of thorium(IV) tungstomolybdate and pectin thorium(IV) tungstomolybdate nanocomposite have been calculated using Tauc relation as

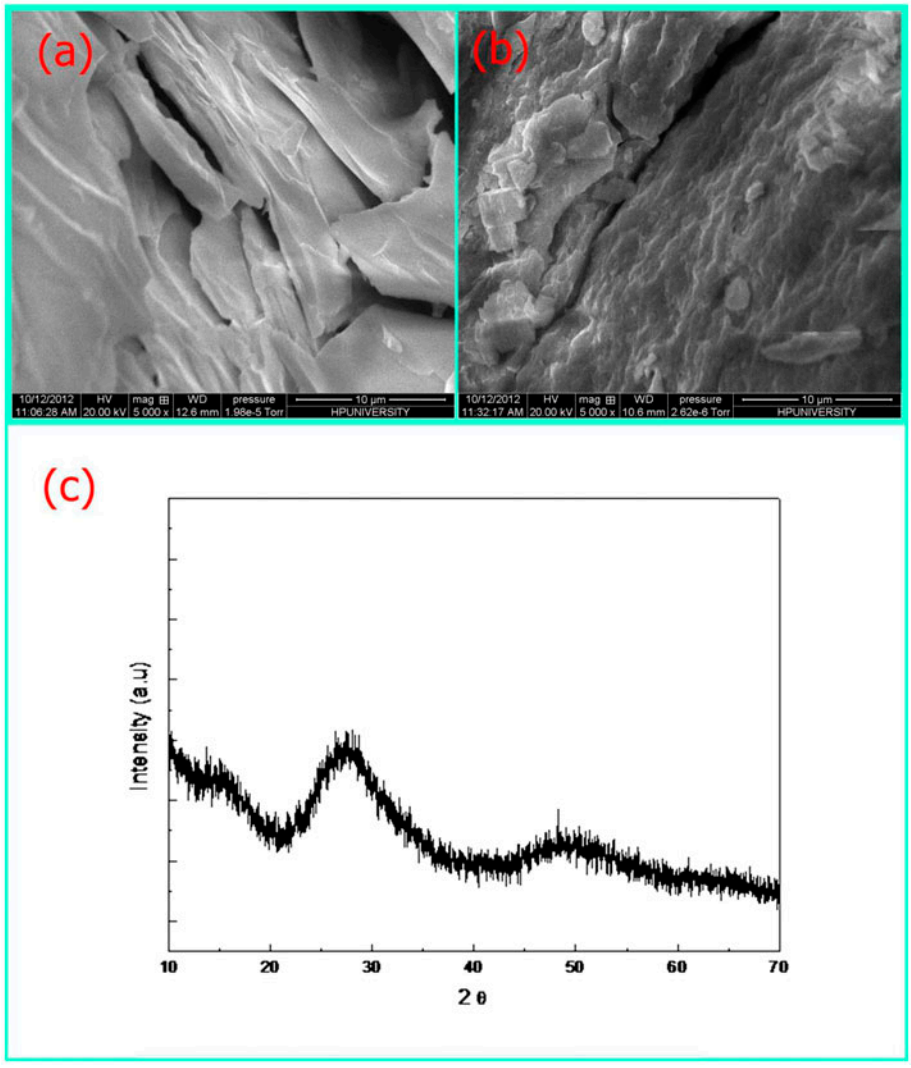


Fig. 2. SEM photographs and (a–b) XRD pattern (c) of pectin thorium(IV) tungstomolybdate [33].

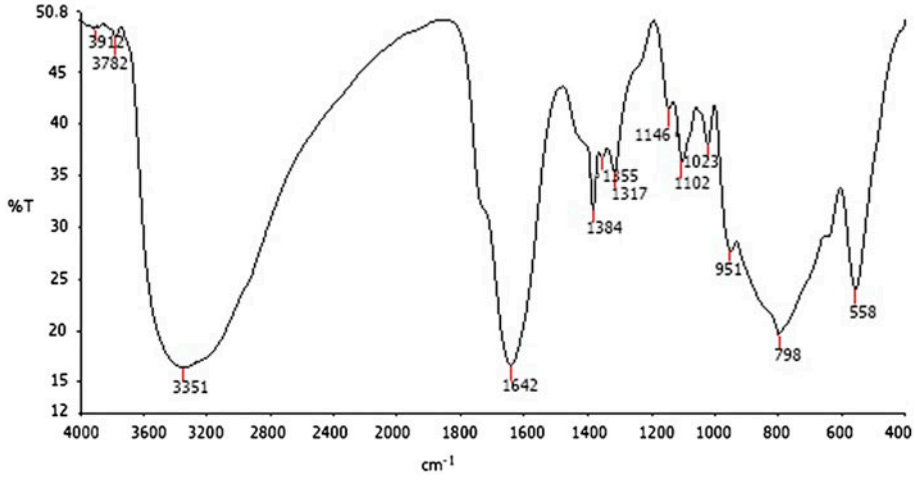


Fig. 3. FTIR spectrum of pectin thorium(IV) tungstomolybdate [33].

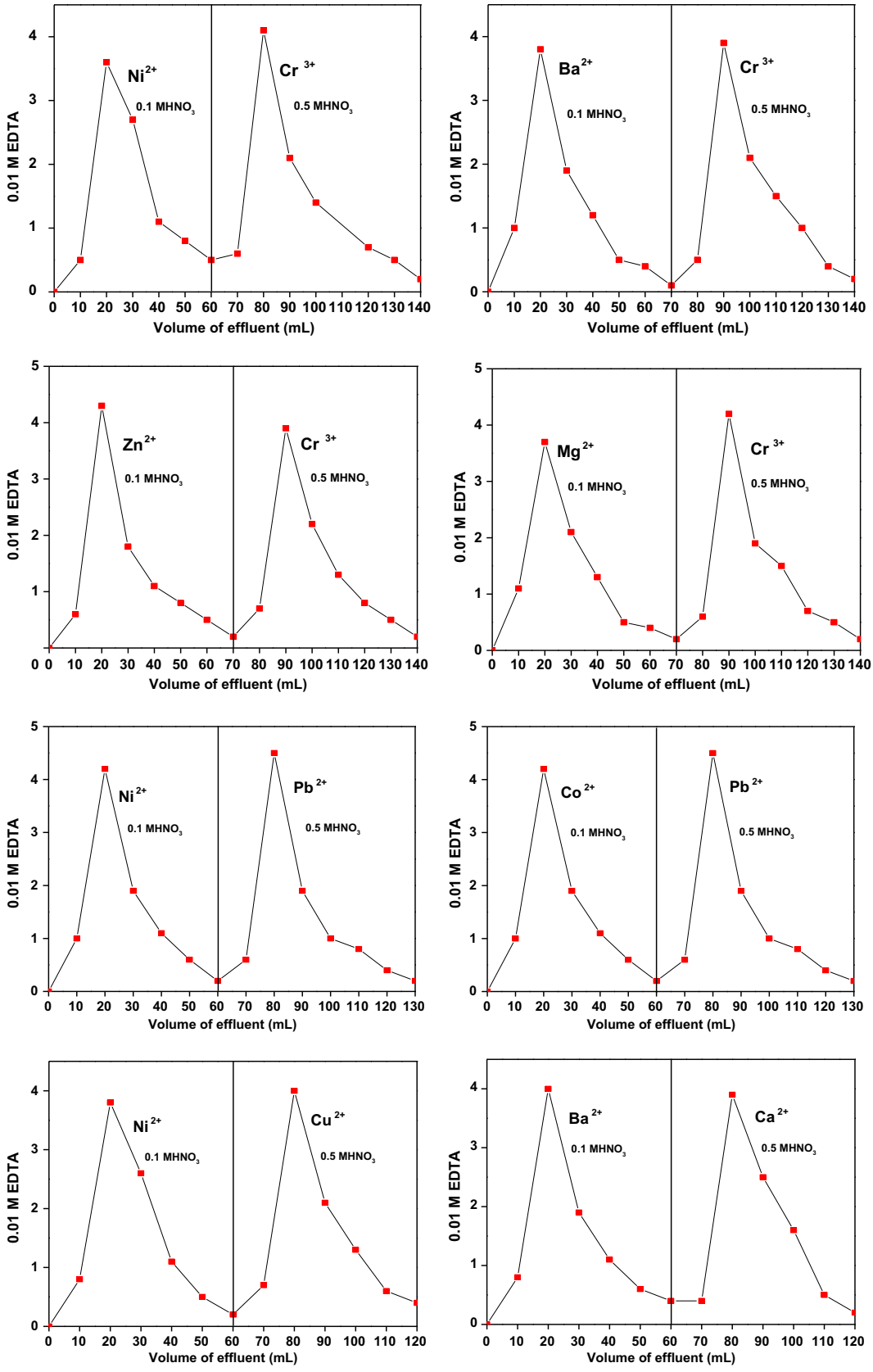


Fig. 4. Chromatograms of binary separations of metal ions on Pc/TWM nanocomposite ion-exchanger column (elutent used 0.1 M and 0.5 M $HNO_3$).

shown in Fig. 6(a) and (b). The band gap as determined from Tauc plots was 3.35 eV for thorium (IV) tungstomolybdate and 3.30 eV for pectin thorium (IV) tungstomolybdate. The band gap of pectin thorium(IV) tungstomolybdate was found lower than thorium(IV) tungstomolybdate, may be due to strong sp-d exchange interactions. Also, the polymer reduces the recombination chance of excitations. The capping induces the distortion of the local electric field and the photo-induced electrons–holes could be trapped around the polymer. The decrease in optical band gap thus enhances the visible region applications of pectin thorium(IV) tungstomolybdate.

### 3.4. Dye removal studies

Fig. 7(a) and (b) shows the photocatalytic degradation of MG dye using pectin thorium(IV) tungstomolybdate nanocomposite under two conditions: (i) equilibrium adsorption in dark followed by photocatalysis and (ii) synergistic adsorptional/photocatalysis directly under sunlight irradiation. The decrease in the adsorption band intensities were observed for MG which clearly revealed that the dye was degraded effectively by pectin thorium(IV) tungstomolybdate nanocomposite.

#### 3.4.1. Equilibrium adsorption in dark followed by photocatalysis

Under dark condition, nanocomposite acted as an absorbent for the adsorption of dye from the water system. The MG dye gets adsorbed onto the nanocomposite, till the adsorption–desorption equilibrium was established. The dye adsorbed nanocomposite with dye solution was exposed to sunlight for further photocatalysis. Fig. 7(a) shows the UV–vis spectral changes of MG with reaction time under visible light. About 29.69% MG dye was absorbed into pectin thorium(IV) tungstomolybdate under dark conditions (Fig. 7(c)). Further, photodegradation of dye in sunlight revealed that 63.43% MG (Fig. 7(c)) removal occurred in 5 h as shown in Table 4.

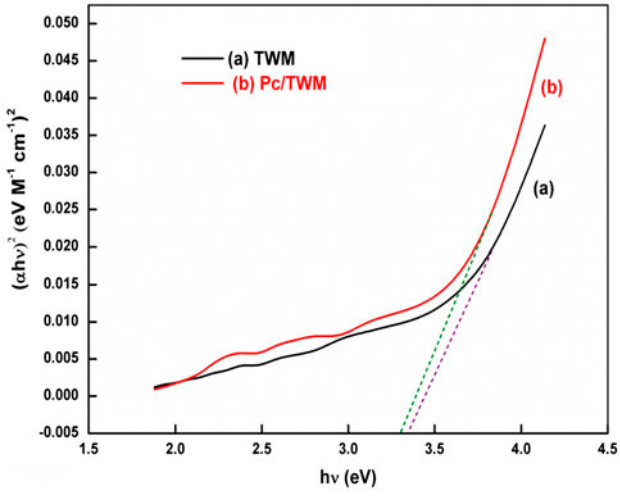


Fig. 5. (a–b) Tauc plots for TWM and Pc/TWM.

The mechanism of equilibrium adsorption followed by photocatalysis is as follows:

First step—Dye (in dark at equilibrium)

$$\text{Pc/TWM} + \text{MG (Free in solution)} \longleftrightarrow \text{Pc/TWM} - \text{MG (adsorbed)}$$

Second step—Adsorption followed by photocatalysis in light

$$\text{Pc/TWM} - \text{MG (adsorbed) and Dye (free in solution)} + h\nu \longrightarrow \text{Pc/TWM}(e^- + \text{h}^+) - \text{MG}$$

$$h^+ + \text{H}_2\text{O} \longrightarrow \text{OH}^* + \text{H}^+$$

$$h^+ + \text{OH}^- \longrightarrow \text{OH}^*$$

$$e^- + \text{O}_2 \longrightarrow \text{O}_2^{-*}$$

$$\text{O}_2^{-*} \text{ or } \text{OH}^* + \text{MG (adsorbed and free in solution)} - \rightarrow \text{Intermediate Product} \longrightarrow \text{Degraded Product}$$

The rate of photocatalytic degradation of various dyes reported followed the pseudo-first-order kinetic model [34,35]:

$$r = -\frac{\mathrm{d}A}{\mathrm{d}t} = k_{\text{app}}t \tag{6}$$

On integrating the above equation, we get:

$$\ln A_o/A_t = k_{\text{app}}t \tag{7}$$

where $k_{\text{app}}$ is the apparent rate constant, $A_o$ is the absorbance of dye before illumination, and $A_t$ is the absorbance of dye at time $t$.

The plot of $\ln A_o/A_t$ vs. irradiation time revealed a linear correlation with good precision as shown in Fig. 7(e). Hence, the photodegradation of MG dye by Pc/TWM nanocomposite was sound fitted to pseudo-first-order kinetics [40,41]. The value of rate constant $k$ for MG (0.00138 min$^{-1}$) was calculated from the slope

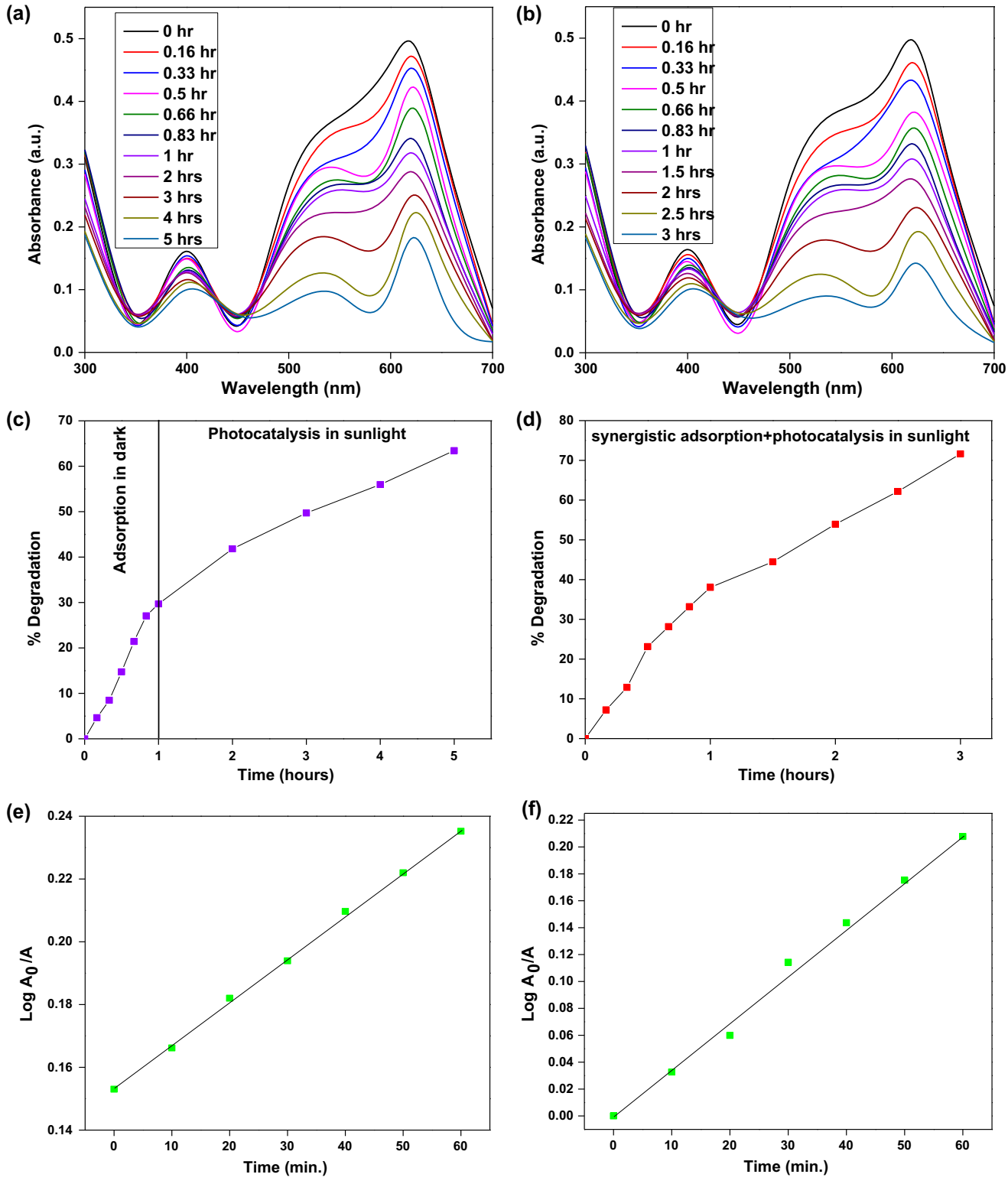


Fig. 6. (i) Spectra of MG (a) equilibrium adsorption in dark followed by photocatalysis (b) synergistic adsorptional/photocatalysis (ii) % degradation of MG (c) equilibrium adsorption in dark followed by photocatalysis (d) synergistic adsorptional/photocatalysis (iii) pseudo-first-order kinetics for MG photodegradation (e) equilibrium adsorption in dark followed by photocatalysis (f) synergistic adsorptional/photocatalysis in presence of Pc/TWM (initial concentration of MG $2 \times 10^{-6}$ M, pH 7, temperature = 30 ± 0.5°C).

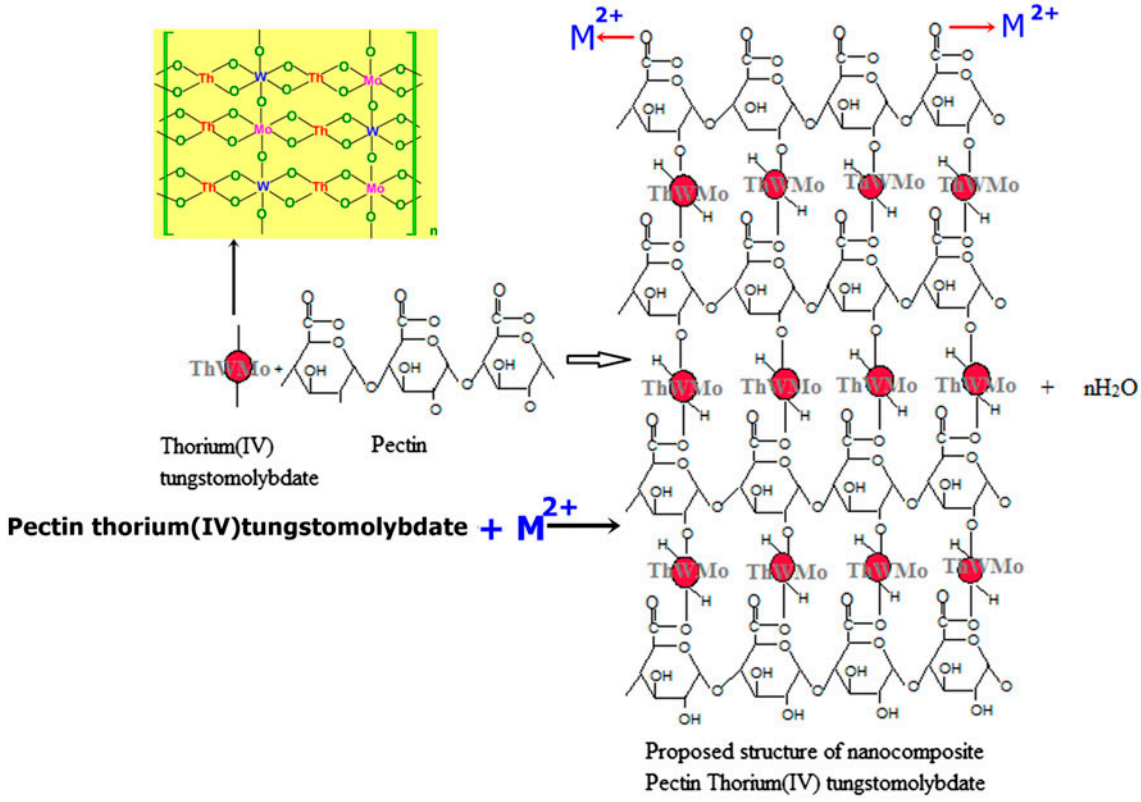


Fig. 7. Adsorption of metal ions onto Pc/TWM nanocomposite [33].

of the plot and the value of correlation coefficient ($R^2$) for MG is shown in Table 4.

The degradation of MG into Pc/TWM nanocomposite was possible due to the presence of transition metals in the composite matrix such as thorium, tungsten, and molybdate. The metal ions are responsible for the generation of electron–hole pair, which leads to disruption of conjugation in dye molecules.

### 3.4.2. *Synergistic adsorptional/photocatalysis directly in sunlight*

Under these conditions, a synergistic effect of adsorption and photocatalysis for the dye degradation was studied. The Fig. 7(b) showed the UV–vis spectral changes with reaction time, showing the extent of degradation of MG during synergistic adsorptional/photocatalysis. The adsorptional/photocatalysis of MG dyes involves the adsorption of dye onto the material and photodegradation of dye molecules at the same time. The transition metals such as tungsten, thorium, and molybdate present in composite matrix produce free radicals [45,46]. The free radicals disrupt the conjugation in the adsorbed and free dye molecules. Thus, degrade the dye. The degraded dye products left the surface of nanocomposite free for further adsorption and photocatalysis. The recommended mechanism for the degradation of dye under synergistic adsorptional/photocatalysis condition is as follows:

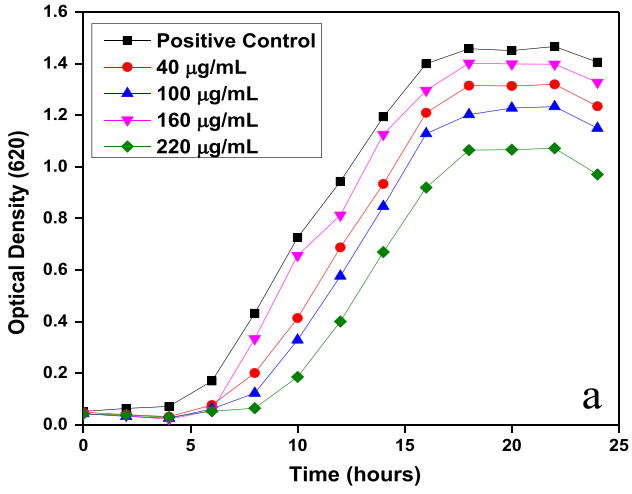


Fig. 8. Growth curve of *S. aureus* in presence of Pc/TWM nanocomposite.

Table 1
Binary separation of metal ions achieved on the Pc/TWM nanocomposite column

| Binary mixtures | Amount loaded (mg) | Amount found[a] (mg) | % Recovery | Eluent used | Volume of eluent required for elution of metal ions (mL) |
|---|---|---|---|---|---|
| $Ni^{2+}$ | 5.86 | 5.39 | 91.98 | 0.1 M $HNO_3$ | 60 |
| $Cr^{3+}$ | 5.19 | 4.98 | 95.95 | 0.5 M $HNO_3$ | 70 |
| $Ba^{2+}$ | 13.73 | 12.21 | 88.93 | 0.1 M $HNO_3$ | 70 |
| $Cr^{3+}$ | 5.19 | 4.98 | 95.95 | 0.5 M $HNO_3$ | 70 |
| $Zn^{2+}$ | 6.53 | 6.07 | 92.95 | 0.1 M $HNO_3$ | 70 |
| $Cr^{3+}$ | 5.19 | 4.98 | 95.95 | 0.5 M $HNO_3$ | 70 |
| $Mg^{2+}$ | 2.43 | 2.25 | 92.59 | 0.1 M $HNO_3$ | 70 |
| $Cr^{3+}$ | 5.19 | 4.98 | 95.95 | 0.5 M $HNO_3$ | 70 |
| $Ni^{2+}$ | 5.86 | 5.39 | 91.97 | 0.1 M $HNO_3$ | 60 |
| $Pb^{2+}$ | 20.72 | 19.47 | 93.97 | 0.5 M $HNO_3$ | 70 |
| $Co^{2+}$ | 5.89 | 5.30 | 89.98 | 0.1 M $HNO_3$ | 60 |
| $Pb^{2+}$ | 20.72 | 19.47 | 93.97 | 0.5 M $HNO_3$ | 70 |
| $Ni^{2+}$ | 5.86 | 5.27 | 89.93 | 0.1 M $HNO_3$ | 60 |
| $Cu^{2+}$ | 6.35 | 5.78 | 91.02 | 0.5 M $HNO_3$ | 60 |
| $Ba^{2+}$ | 13.73 | 12.08 | 87.98 | 0.1 M $HNO_3$ | 60 |
| $Ca^{2+}$ | 4.00 | 3.64 | 91.00 | 0.5 M $HNO_3$ | 60 |

[a]Average of three replicate determinations.

Table 2
Selective separation of $Cr^{3+}$ from a synthetic mixture of $Cr^{3+}$, $Zn^{2+}$, $Ni^{2+}$, $Pb^{2+}$, $Sr^{2+}$, $Mg^{2+}$, and $Cd^{2+}$ on the column of Pc/TWM nanocomposite

| Metal ion | Amount loaded (mg) | Amount found[a] (mg) | % Recovery | % Error | Volume of eluent used | Eluent used |
|---|---|---|---|---|---|---|
| $Cr^{3+}$ | 0.51 (Set-1) | 0.49 | 96.08 | −3.92 | 70 | 0.5 M Nitric acid |
| | 1.02 (Set-2) | 1.23 | 97.06 | −2.94 | 70 | |
| | 2.04 (Set-3) | 1.97 | 96.57 | −3.43 | 70 | |

[a]Average of three replicate determinations.
Notes: The selective separation of $Cr^{3+}$ has been attempted from the synthetic mixture of different metal ions in three different sets as:
Set 1: $Cr^{3+}$ (0.51 mg), $Zn^{2+}$ (0.65 mg), $Ni^{2+}$ (0.58 mg), $Pb^{2+}$ (2.07 mg), $Sr^{2+}$ (0.88 mg), $Mg^{2+}$ (0.24 mg), and $Cd^{2+}$ (1.12 mg).
Set 2: $Cr^{3+}$ (1.02 mg) and the amount of other metals was kept same as taken in set 1.
Set 3: $Cr^{3+}$ (2.04 mg) and the amount of other metals was kept same as taken in set 1.

$$\mathrm{Pc/TWM} + \mathrm{MB\ Dye\ adsorbed} \longleftrightarrow \mathrm{Pc/TWM} - \mathrm{Dye\ absorbed\ (in\ sunlight)}$$

$$\mathrm{Pc/TWM}\,(h^+) - \mathrm{Dye\ adsorbed} + \mathrm{H_2O} - \rightarrow \mathrm{Pc/TWM}\,(\mathrm{OH}^*) - \mathrm{Dye} + \mathrm{H}^+$$

$$\mathrm{Pc/TWM}\,(h^+) - \mathrm{Dye\ adsorbed} + \mathrm{OH}^- - \rightarrow \mathrm{Pc/TWM}\,(\mathrm{OH}^*) - \mathrm{Dye}$$

$$\mathrm{Pc/TWM}\,(e^-) - \mathrm{Dye\ adsorbed} + \mathrm{O_2} - \rightarrow \mathrm{Pc/TWM}\,(\mathrm{O_2^{-*}}) - \mathrm{Dye}$$

$$\mathrm{O_2^{-*}\ or\ OH^*} + \mathrm{Dye} - \mathrm{Pc/ZSWP} - \rightarrow \mathrm{Intermediate\ Product} - \rightarrow \mathrm{Degraded\ Product} + \mathrm{Free\ Pc/TWM\ for\ reuse}$$

It has been observed that about 71.62% MG (Fig. 7(d)) dye was removed in 3 h of photoperiod under synergistic adsorptional/photocatalysis condition as shown in Table 5. The whole process of dye degradation followed a pseudo-first-order kinetics with an overall rate constant ($k_o$) (Table 5) 0.00354 $min^{-1}$ for MG (Fig. 7(f)). The values of correlation coefficient ($R^2$) for MG under synergistic adsorptional/photocatalysis condition are shown in Table 5. The

Table 3
Selective separation of $Pb^{2+}$ from a synthetic mixture of $Pb^{2+}$, $Zn^{2+}$, $Ni^{2+}$, $Al^{3+}$, $Co^{2+}$, $Mg^{2+}$, and $Fe^{3+}$ on the column of Pc/TWM nanocomposite

| Metal ion | Amount loaded (mg) | Amount found[a] (mg) | % Recovery | % Error | Volume of eluent used | Eluent used |
|---|---|---|---|---|---|---|
| $Pb^{2+}$ | 1.35 (Set-1) | 1.28 | 94.81 | −5.19 | 70 | 0.5 M Nitric acid |
| | 2.07 (Set-2) | 1.97 | 95.17 | −4.83 | 70 | |
| | 4.14 (Set-3) | 3.98 | 96.13 | −3.87 | 70 | |

[a]Average of three replicate determinations.
Notes: The selective separation of $Pb^{2+}$ has been attempted from the synthetic mixture of different metal ions in three different sets as:
Set 1: $Pb^{2+}$ (1.35 mg), $Zn^{2+}$ (0.65 mg), $Ni^{2+}$ (0.58 mg), $Al^{3+}$ (0.27 mg), $Co^{2+}$ (0.58 mg), $Mg^{2+}$ (0.24 mg), and $Fe^{3+}$ (0.56 mg).
Set 2: $Pb^{2+}$ (2.07 mg) and the amount of other metals was kept same as taken in set 1.
Set 3: $Pb^{2+}$ (4.14 mg) and the amount of other metals was kept same as taken in set 1.

Table 4
% Removal of MG by Pc/TWM under two reaction conditions: equilibrium adsorption followed by photocatalysis and synergistic adsorptional/photocatalysis

| Dye | | For adsorption followed by photocatalysis | | For synergistic adsorptional/photocatalysis |
|---|---|---|---|---|
| | Concentration (M) | % adsorption (in 1 h) in Dark | % degradation (in 5 h) in sunlight | % removal of dye |
| MG | $2 \times 10^{-6}$ | 29.69 | 63.43 | 71.62 |

Table 5
Apparent rate constants and linear regression coefficients from log $A_o/A$ vs. $T$ plots for MG in presence of Pc/TWM

| Dye | | For adsorption followed by photocatalysis | | For synergistic adsorptional/photocatalysis | |
|---|---|---|---|---|---|
| | Concentration (M) | $k_{app}$ ($min^{-1}$) | $R^2$ | $k_{app}$ ($min^{-1}$) | $R^2$ |
| MG | $2 \times 10^{-6}$ | 0.00138 | 0.9988 | 0.00354 | 0.9929 |

rate constants clearly revealed the higher rate of photodegradation under synergistic adsorptional/photocatalysis reaction conditions.

It has been shown that the degradation of MG dye proceeded faster under synergistically adsorptional/photocatalysis conditions compared to equilibrium adsorption in the dark followed by photocatalysis within 3 h of photoperiod. The reason behind this degradation is same as for Pc/ZSWP nanocomposite. As under synergistic process conditions, the adsorption and photocatalysis work together at the same time. The polymeric part pectin is responsible for absorption of dyes from solution and at the same time transition metals generate the electron–hole pairs on absorption of light which results in photodegradation of dye molecules present on surface of material and in solution. The adsorption of dye onto adsorbent facilitates the photodegradation process and reduces the degradation time. The absorbed dye molecules were more susceptible to the attack of radicals than the dye molecules present in the solution.

The comparison of rate constants of synergistic adsorptional/photocatalysis and equilibrium adsorption followed by photocatalysis also reveals that (Table 5) the dye degradation under synergistic conditions was more efficient and effective.

### 3.5. Antimicrobial activity of Pc/TWM nanocomposite

The antimicrobial activity of the nanocomposite Pc/TWM was studied against *S. aureus* by employing O.D method. The growth curves for inhibition of bacteria is shown in Fig. 8. The growth curve studies of *S. aureus* show that Pc/TWM nanocomposite was effective in the destruction of *S. aureus*. It was observed that a concentration of 220 μg/mL Pc/TWM

totally inhibited the growth of *S. aureus* for the 24-h period of incubation. The other concentration of Pc/TWM was also effective in inhibiting the growth of bacteria but to a lesser extent. The death phase of the *S. aureus* was observed after 20 h of incubation. The metal ion present in the nanocomposite was responsible for lysis of bacterial cells. The chemical interactions between the reactive surfaces of Pc/TWM nanocomposite and bacterial cells may be responsible for the disruption of the cell membrane. The induced reductive decomposition of functional groups in the proteins and lipopolysaccharides of the outer membranes may also be responsible for killing the bacteria [47].

## 4. Conclusion

The pectin thorium(IV) tungstomolybdate nanocomposite has been examined for its efficiency in metal separation and degradation of malachite green dye from water. It was found that the nanocomposite is a multifunctional material which can be employed for environmental remediation.

## Acknowledgments

We acknowledge Department of Chemistry, Shoolini University for providing necessary facilities. One of the authors (Mu. Naushad) would like to extend his sincere appreciation to the Deanship of Scientific Research at King Saud University for funding this work through the Research Group No. RG-1436-034.

## References

[1] M. Lasindrang, H. Suwarno, S.D. Tandjung, H.N. Kamiso, Adsorption pollution leather tanning industry wastewater by chitosan coated coconut shell active charcoal, Agric. Agric. Sci. Procedia 3 (2015) 241–247.
[2] Y-J. Tu, C-F. You, C-K. Chang, S-L. Wang, T-S. Chan, Adsorption behavior of As(III) onto a copper ferrite generated from printed circuit board industry, Chem. Eng. J. 225 (2013) 433–439.
[3] S-M. Alatalo, E. Repo, E. Mäkilä, J. Salonen, E. Vakkilainen, M. Sillanpää, Adsorption behavior of hydrothermally treated municipal sludge & pulp and paper industry sludge, Bioresour. Technol. 147 (2013) 71–76.
[4] O. Ashrafi, L. Yerushalmi, F. Haghighat, Wastewater treatment in the pulp-and-paper industry: A review of treatment processes and the associated greenhouse gas emission, J. Environ. Manage. 158 (2015) 146–157.
[5] M.R. Awual, M.M. Hasan, A. Shahat, M. Naushad, H. Shiwaku, T. Yaita, Investigation of ligand immobilized nano-composite adsorbent for efficient cerium(III) detection and recovery, Chem. Eng. J. 265 (2015) 210–218.
[6] D. Pathania, G. Sharma, R. Thakur, Pectin @ zirconium (IV) silicophosphate nanocomposite ion exchanger: Photocatalysis, heavy metal separation and antibacterial activity, Chem. Eng. J. 267 (2015) 235–244.
[7] Mu. Naushad, Z.A. ALOthman, G. Sharma, Inamuddin, Kinetics, isotherm and thermodynamic investigations for the adsorption of Co(II) ion onto crystal violet modified amberlite IR-120 resin, Ionics 21 (2014) 1453–1459.
[8] A.A. Khan, A. Khan, Ion-exchange studies on poly-o-anisidine Sn(IV) phosphate nano composite and its application as Cd(II) ion-selective membrane electrode, Centr. Eur. J. Chem. 8 (2010) 396–408.
[9] S. Amirnia, M.B. Ray, A. Margaritis, Heavy metals removal from aqueous solutions using *Saccharomyces cerevisiae* in a novel continuous bioreactor–biosorption system, Chem. Eng. J. 264 (2015) 863–872.
[10] V.K. Gupta, T.A. Saleh, D. Pathania, B.S. Rathore, G. Sharma, A cellulose acetate based nanocomposite for photocatalytic degradation of methylene blue dye under solar light, Ionics 21 (2015) 1787–1793.
[11] R. Katwal, H. Kaur, G. Sharma, M. Naushad, D. Pathania, Electrochemical synthesized copper oxide nanoparticles for enhanced photocatalytic and antimicrobial activity, J. Ind. Eng. Chem. 31 (2015) 173–184.
[12] J.G. Yu, L.Y. Yu, H. Yang, Q. Liu, X.H. Chen, X.Y. Jiang, X.Q. Chen, F.P. Jiao, Graphene nanosheets as novel adsorbents in adsorption, preconcentration and removal of gases, organic compounds and metal ions, Sci. Total Environ. 502 (2015) 70–79.
[13] A. Kumar, G. Sharma, M. Naushad, S. Thakur, SPION/β-cyclodextrin core-shell nanostructures for oil spill remediation and organic pollutant removal from waste water, Chem. Eng. J. 280 (2015) 175–187.
[14] G. Sharma, M. Naushad, D. Pathania, A. Mittal, G.E. El-desoky, Modification of *Hibiscus cannabinus* fiber by graft copolymerization: application for dye removal, Desalin. Water Treat. 54 (2015) 3114–3121.
[15] A.A. Khan, M.M. Alam, New and novel organic–inorganic type crystalline 'polypyrrolel/polyantimonic acid' composite system: Preparation, characterization and analytical applications as a cation-exchange material and Hg(II) ion-selective membrane electrode, Anal. Chim. Acta 504 (2004) 253–264.
[16] D. Pathania, G. Sharma, M. Naushad, V. Priya, A biopolymer-based hybrid cation exchanger pectin cerium (IV) iodate: Synthesis, characterization, and analytical applications, Desalin. Water Treat. 1–8, doi: 10.1080/19443994.2014.967731.
[17] Z.A. ALothman, Inamuddin, M. Naushad, Adsorption thermodynamics of trichloroacetic acid herbicide on polypyrroleTh(IV) phosphate composite cation-exchanger, Chem. Eng. J. 169 (2011) 38–42.
[18] M. Islam, R. Patel, Polyacrylamide thorium(IV) phosphate as an important lead selective fibrous ion exchanger: Synthesis, characterization and removal study, J. Hazard. Mater. 156 (2008) 509–520.
[19] Z.A. ALothman, Inamudin, M. Naushad, Organic–inorganic type composite cation exchanger poly-o-toluidine Zr(IV) tungstate: Preparation, physicochemical characterization and its analytical application in separation of heavy metals, Chem. Eng. J. 172 (2011) 369–375.

[20] S.A. Nabi, M. Naushad, Synthesis, characterization and analytical applications of a new composite cation exchanger cellulose acetate-Zr(IV) molybdophosphate, Colloids and Surf., A: Physicochem. Eng. Aspects 316 (2008) 217–225.
[21] V.K. Gupta, D. Pathania, N.C. Kothiyal, G. Sharma, Polyaniline zirconium(IV) silicophosphate nanocomposite for remediation of methylene blue dye from waste water, J. Mol. Liq. 190 (2014) 139–145.
[22] M. Naushad, Surfactant assisted nano-composite cation exchanger: Development, characterization and applications for the removal of toxic $Pb^{2+}$ from aqueous medium, Chem. Eng. J. 235 (2014) 100–108.
[23] X.H. Zhao, F.P. Jiao, J.G. Yu, Y. Xi, X.Y. Jiang, X.Q. Chen, Removal of Cu(II) from aqueous solutions by tartaric acid modified multi-walled carbon nanotubes, Colloids Surf., A: Physicochem. Eng. Aspects 476 (2015) 35–41.
[24] B.S. Rathore, G. Sharma, D. Pathania, V.K. Gupta, Synthesis, characterization and antibacterial activity of cellulose acetate–tin(IV) phosphate nanocomposite, Carbohydr. Polym. 103 (2014) 221–227.
[25] A. Clearfield, Inorganic Ion Exchange Materials, CRC Press, Boca Raton, Florida, 1982.
[26] A.A. Khan, Inamuddin, M.M. Alam, Preparation, characterization and analytical applications of a new and novel electrically conducting fibrous type polymeric–inorganic composite material: Polypyrrole Th (IV) phosphate used as a cation-exchanger and Pb(II) ion-selective membrane electrode, Mater. Res. Bull. 40 (2005) 289–305.
[27] A.A. Khan, R. Niwas, M.M. Alam, Ion-exchange kinetics on styrene supported zirconium(IV) tungstophosphate: An organic-inorganic type cation exchanger, Indian. J. Chem. Technol. 9 (2002) 256–260.
[28] S.A. Nabi, M. Naushad, R. Bushra, Synthesis and characterization of a new organic–inorganic $Pb^{2+}$ selective composite cation exchanger acrylonitrile stannic(IV) tungstate and its analytical applications, Chem. Eng. J. 152 (2009) 80–87.
[29] G. Sharma, D. Pathania, M. Naushad, Preparation, characterization and antimicrobial activity of biopolymer based nanocomposite ion exchanger pectin zirconium (IV) selenotungstophosphate: Application for removal of toxic metals, J. Ind. Eng. Chem. 20 (2014) 4482–4490.
[30] V.K. Gupta, D. Pathania, M. Asif, G. Sharma, Liquid phase synthesis of pectin–cadmium sulfide nanocomposite and its photocatalytic and antibacterial activity, J. Mol. Liq. 196 (2014) 107–112.
[31] S.A. Nabi, M. Shahadat, R. Bushra, A.H. Shalla, F. Ahmed, Development of composite ion-exchange adsorbent for pollutants removal from environmental wastes, Chem. Eng. J. 165 (2010) 405–412.
[32] O. Arrad, Y. Sasson, Commercial ion exchange resins as catalysts in solid-solid-liquid reactions, J. Org. Chem. 54 (1989) 4993–4998.
[33] V.K. Gupta, S. Agarwal, D. Pathania, N.C. Kothiyal, G. Sharma, Use of pectin–thorium(IV) tungstomolybdate nanocomposite for photocatalytic degradation of methylene blue, Carbohydr. Polym. 96 (2013) 277–283.
[34] R. Seoudi, A.B. El-Bailly, W. Eisa, A.A. Shabaka, S.I. Soliman, R.K. Abd El, R.A. Romadan, Synthesis, optical and dielectric properties of (PVA/CdS) nanocomposites, J. Appl. Sci. Res. 8 (2012) 658–667.
[35] M.L. Dinesha, H.S. Jayanna, S. Mohanty, S. Ravi, Structural, electrical and magnetic properties of Co and Fe co-doped ZnO nanoparticles prepared by solution combustion method, J. Alloys Compd. 490 (2010) 618–623.
[36] S.L. Patil, S.G. Pawar, A.T. Mane, Nanocrystalline ZnO thin films: Optoelectronic and gas sensing properties, J. Mater. Sci. Mater. Electr. 21 (2010) 1332–1336.
[37] C.N. Reilley, R.W. Schmid, F.S. Sadek, Chelon approach to analysis: I. Survey of theory and application, J. Chem. Educ. 36 (1959) 555–564.
[38] G. Sharma, D. Pathania, M. Naushad, N.C. Kothiyal, Fabrication, characterization and antimicrobial activity of polyaniline Th(IV) tungstomolybdophosphate nanocomposite material: Efficient removal of toxic metal ions from water, Chem. Eng. J. 251 (2014) 413–421.
[39] S. Liu, H. Sun, S. Liu, S. Wang, Graphene facilitated visible light photodegradation of methylene blue over titanium dioxide photocatalysts, Chem. Eng. J. 214 (2013) 298–303.
[40] A.V. Rupa, D. Manikandan, D. Divakar, T. Sivakumar, Effect of deposition of Ag on $TiO_2$ nanoparticles on the photodegradation of Reactive Yellow-17, J. Hazard. Mater. 147 (2007) 906–913.
[41] J. Xu, Y. Ao, D. Fu, C. Yuan, Low-temperature preparation of F-doped $TiO_2$ film and its photocatalytic activity under solar light, Appl. Surf. Sci. 254 (2008) 3033–3038.
[42] M. Sadiq, B. Chowdhury, N. Chandrasekaran, A. Mukherjee, Antimicrobial sensitivity of *Escherichia coli* to alumina nanoparticles, Nanomed. Nanotechnol. Biol. Med. 5 (2005) 282–286.
[43] W. Rizwan, M. Amrita, H. Soon-Il, K.Y. Soon, S.J. Hyng-shik, Antibacterial activity of ZnO nanoparticles prepared via non-hydrolytic solution route, Appl. Microbio. Biotechnol. 87 (2010) 1917–1925.
[44] D.N. Williams, S.H. Ehrman, T.R.P. Holoman, Evaluation of the microbial growth response to inorganic nanoparticles, J. Nanobiotechnol. 4 (2006) 3–6.
[45] M. Sanchez-Polo, M.M. Abdeldaiem, R. Ocampo-Perez, J. Rivera-Utrilla, A.J. Mota, Comparative study of the photodegradation of bisphenol A by $HO_2SO^{4-}$ and $CO^{3-}/HCO_3$ radicals in aqueous phase, Sci. Total Environ. 463–464 (2013) 421–431.
[46] M.S. Hamdy, W.H. Saputera, E.J. Groenen, G. Mul, A novel $TiO_2$ composite for photocatalytic wastewater treatment, J. Appl. Sci. Res. 8 (2014) 658–662.
[47] D. Pathania, G. Sharma, M. Naushad, A. Kumar, Synthesis and characterization of a new nanocomposite cation exchanger polyacrylamide Ce(IV) silicophosphate: Photocatalytic and antimicrobial applications, J. Ind. Eng. Chem. 20 (2014) 3596–3603.